Transendothelial migration induces differential migration dynamics of leukocytes in tissue matrix

Abraham C.I. van Steen[1,*], Lanette Kempers[1,*], Rouven Schoppmeyer[1,3], Max Blokker[2], David J. Beebe[4], Martijn A. Nolte[1] and Jaap D. van Buul[1,3,+]

[1] Department of Molecular Hematology, Sanquin Research, Amsterdam, The Netherlands
[2] Department of Physics, Vrije Universiteit Amsterdam, Amsterdam, The Netherlands.
[3] Leeuwenhoek Centre for Advanced Microscopy (LCAM), section Molecular Cytology at Swammerdam Institute for Life Sciences (SILS) at University of Amsterdam, The Netherlands.
[4] Department of Biomedical Engineering Department of Pathology and Laboratory Medicine, Carbone Cancer Center, University of Wisconsin-Madison, Madison, WI

*** These authors contributed equally.**

+Correspondence should be addressed to:

Jaap D. van Buul

Molecular Cell Biology Lab, Dept. Molecular Hematology

Sanquin Research and Landsteiner Laboratory

Academic Medical Center at the University of Amsterdam

Plesmanlaan 125, 1066CX Amsterdam, the Netherlands

Phone: +31205123042

E-mail: j.vanbuul@sanquin.nl

Keywords: Leukocyte transendothelial migration, endothelial cells, inflammation, blood-vessel-on-a-chip, tissue, extracellular matrix, physiological hydrogel, blood vessels, migration dynamics.

Summary

A functional hydrogel-based blood-vessel-on-a-chip model is used to study the complete leukocyte transendothelial migration process in real time. T-lymphocytes and neutrophils exhibit distinct migration dynamics in the extravascular matrix after transendothelial migration, which can be altered using a chemotactic gradient.

Abstract

Leukocyte extravasation into inflamed tissue is a complex process that is difficult to capture as a whole *in vitro*. We employed a blood-vessel-on-a-chip model in which endothelial cells were cultured in a tube-like lumen in a collagen-1 matrix. The vessels are leak-tight, creating a barrier for molecules and leukocytes. Addition of inflammatory cytokine TNF-α caused vasoconstriction, actin remodelling and upregulation of ICAM-1. Introducing leukocytes into the vessels allowed real-time visualisation of all different steps of the leukocyte transmigration cascade including migration into the extracellular matrix. Individual cell tracking over time distinguished striking differences in migratory behaviour between T-cells and neutrophils. Neutrophils cross the endothelial layer more efficiently than T-cells, but upon entering the matrix, neutrophils display high speed but low persistence, whereas T-cells migrate with low speed and rather linear migration. In conclusion, 3D imaging in real-time of leukocyte extravasation in a vessel-on-a-chip enables detailed qualitative and quantitative analysis of different stages of the full leukocyte extravasation process in a single assay.

Introduction

Leukocyte transendothelial migration (TEM) forms the basis of immune surveillance and pathogen clearance, and hence plays a pivotal role in many (patho)physiological processes. This process is highly regulated and strongly differs between the various leukocyte subsets and tissues involved. Leukocyte extravasation mainly occurs in postcapillary venules, where adherens junctions allow for transient opening of the barrier to allow leukocytes to pass.

Importantly, most venules only allow leukocyte TEM when the surrounding tissue is inflamed, thereby locally exposed to pro-inflammatory cytokines. One of those is tumour Necrosis Factor-α (TNF-α), which is produced by a variety of cells under inflammatory conditions (Heller and Krönke, 1994). Once leukocytes have crossed the endothelial barrier, they continue migrating into the underlying matrix to fight the invading pathogens (Woodfin, Voisin and Nourshargh, 2010). Tissue penetration is an important aspect of the extravasation process as this determines if a pathogen will be successfully cleared or not (Yamada and Sixt, 2019). It is therefore essential to understand how immune cells migrate through the extracellular matrix once they have crossed the endothelium. To date, the full extravasation process, including intraluminal rolling, crawling, diapedesis and the extracellular 3D matrix migration, can only be studied using *in vivo* models as no proper *in vitro* models are available. As *in vivo* models have their limitations, it would be more than desirable to have an *in vitro* system that allow to study the full process in real-time.

Research regarding the TEM process on a cellular level is mainly done using 2D *in vitro* models, generally based on endothelial cell monolayers cultured on flat stiff surfaces, such as coverslips (Muller and Luscinskas, 2008). Substrate stiffness has been shown to affect cell-cell and cell-matrix interactions of endothelial cells, as well as leukocyte–endothelial cell interactions, and subsequently TEM (Huynh *et al.*, 2011; Stroka and Aranda-Espinoza, 2011). Another limitation is that leukocytes encounter this stiff impermeable surface after traversing the endothelial barrier, making it impossible to study leukocyte detachment from the vessel and entry into the tissue. 3D systems, such as Transwell assays and Boyden chamber assays, allow leukocytes to advance beyond the endothelial cell monolayer, however these systems are unsuitable for microscopy-based imaging and are also based on stiff substrates (Muller and Luscinskas, 2008). To achieve the next step in TEM research, a more intricate model is required that allows imaging of the entire process from the luminal side of the endothelium into a physiological matrix substrate.

Organ-on-a-chip (OOAC) models use microfluidics-based approaches to create biomimetic systems emulating physiological organ function. Blood vessels are well suited for OOAC development, as their structure is relatively simple compared to entire organs (Virumbrales-Muñoz

53 *et al.*, 2020). Knowledge on vascularisation of *in vitro* systems obtained from Blood-Vessel-on-a-Chip
54 (BVOAC) models could also be applied to organoids to overcome their current size and function
55 limitations. BVOAC systems typically consist of a tubular EC monolayer generated in a stiff
56 glass/plastic substrate (Farahat *et al.*, 2012; Zervantonakis *et al.*, 2012; Zheng *et al.*, 2012) or
57 hydrogel (Wong *et al.*, 2012; Kim *et al.*, 2016; Sobrino *et al.*, 2016). A perfusable and hydrogel-based
58 BVOAC system overcomes the aberrations associated with stiff substrates and in addition allows
59 leukocytes to extravasate into the matrix surrounding the vessel.

60 A system that meets these requirements is the LumeNext system, which is also highly suited
61 for imaging analysis (Jiménez-Torres *et al.*, 2016). Apart from building a 3D blood vessel in a
62 physiological matrix, this device allowed us to track the subsequent migration of primary human
63 neutrophils as well as T-cells beyond the diapedesis stage into the matrix in real-time using confocal
64 microscopy. We discovered that neutrophils and T-Lymphocytes use markedly different migration
65 modes to enter the tissue. Moreover, by applying a chemotactic gradient of complement component
66 5a (C5a) into the hydrogel matrix, we found that C5a did not increase the number of neutrophils that
67 crossed the endothelium, but rather promoted migration towards C5a by adjusting directionality of
68 cell migration, while reducing migration speed. These findings demonstrate that the combination of
69 cutting-edge BVOAC systems with advanced microscopy offers valuable new insights into how
70 different leukocyte subsets respond to chemokines and cross the vascular barrier and enter the
71 tissue.

Results

Characterization of endothelium-lined blood vessels

To study leukocyte TEM in a reproducible BVOAC device and monitor this in real time, we used the LumeNext device (Figure 1A) (Jiménez-Torres *et al.*, 2016). Endothelial cells were seeded in the lumen inside a collagen-1 matrix using a head-over-head incubator, allowing the formation of a 3D vessel (Figure 1B). Staining of VE-cadherin, F-actin and nuclei showed the formation of a confluent endothelial monolayer (Figure 1C), as well as a vascular lumen (Figure 1D). Detailed imaging showed a confluent endothelial monolayer with linear junctions, marked by VE-cadherin and F-actin, representative for a functional barrier (Figure 1E) (Ando *et al.*, 2013).

As the barrier function of endothelial monolayers is an essential function of blood vessels, we measured the barrier function in the BVOAC model by perfusing the lumen with fluorescently-labelled 70 kDa dextran, comparable size to albumin, an abundant plasma protein. In a non-vascularized lumen (i.e., no endothelial lining), dextran rapidly diffused into the matrix, whereas in endothelialised lumen, dextran was contained for more than 20 min without leakage. Addition of thrombin, a well-known vascular permeability factor (Van Nieuw Amerongen *et al.*, 1998) to the lumen temporally induced endothelial permeability that recovered over time (Figure 1F-G). This shows that the vessels are functionally lined with endothelial cells and provide a proper barrier function.

BVOAC under inflammatory conditions

Upon inflammation the endothelium upregulates crucial adhesion molecules and chemokines required for leukocyte extravasation. Therefore, we incubated the vessels overnight with the inflammatory mediator TNF-α to activate the endothelial cells (Figure 2A-B). Interestingly, TNF-α did not alter the number of endothelial cells in the BVOAC (Figure 2C) but did lead to a smaller vessel diameter 24 hours after addition of TNF-α (Figure 2D). TNF-α treatment resulted in the induction of actin stress fibres through the cell body and the upregulation of ICAM-1 (Figure 2E). In untreated cells, F-actin was predominantly present at the cell junctions where they colocalised with VE-cadherin. In TNF-α treated cells, cytosolic actin stress fibres are observed in addition to junctional actin stress fibres (Figure 2F). In addition, the endothelial cells produced a layer of Collagen IV around the vessel, making up a basement membrane (Figure 2G). In the orthogonal view, it can be observed that the Collagen IV is present at the baso-lateral side of the endothelium (Figure 2H). The reduced vessel size, upregulation of ICAM-1, increased stress fibre formation and presence of Collagen IV around the vessel illustrate that the endothelial cells were in an inflamed state after TNF-α treatment.

106 **3D analysis of leukocyte transmigration in vessels**

107 Next, we investigated TEM of neutrophils in the BVOAC model. Neutrophils were injected
108 into uninflamed and inflamed vessels and incubated for 2.5 hours. The devices were then washed to
109 remove non-adherent neutrophils, fixed, and imaged using confocal microscopy. We found that
110 neutrophils not only crossed the endothelial monolayer but also continued migration into the
111 underlying collagen matrix (Figure 3A). Imaris software was used to generate a 3D rendering of the
112 BVOAC, which revealed neutrophils mostly transmigrated at the bottom of the vessel (Figure 3B) due
113 to gravity. When allowing transmigration during continuous turning of the device, thereby reducing
114 the effect of local gravity, we found that neutrophils left the vessels at all sides (Figure S1). This
115 rendering was adapted for analysis by manually creating a surface at the position of the vessel
116 (Figure 3C) and creating spots at the centre of mass for neutrophils (Figure 3D), based on automatic
117 detection and manual curation. Following this analysis step, we were able to calculate the distance
118 between the surface and the individual spots who were then colour coded, with warm colours
119 representing longest distance from the endothelium into the matrix (Figure 3E). This analysis allowed
120 us to distinguish between the different steps of TEM, namely adhesion, diapedesis, and penetration
121 into the ECM (Figure 3G). To demonstrate the three different steps of the TEM cascade, we imaged in
122 more detail the wall of the vessel and were able to observe the full TEM process, i.e., rolling,
123 adhesion, and diapedesis (Figure 3H, Supplemental Video 1-2). In the video 2 neutrophils
124 transmigrate at the same spot, shortly after each other, indicating the possible presence of a
125 transmigration hotspot (Grönloh, Arts and van Buul, 2021). Quantification showed that the distance
126 neutrophils travelled from the vessels into the matrix ranging from -18 µm (in the lumen) to 286 µm
127 into the matrix (Figure 3F). Neutrophils with a distance of ≤ 8 µm from the vessel were still adhering
128 to the endothelium. From these data, we conclude that this new analysis tool can track individual
129 neutrophils at all stages of TEM, comparable with *in vivo* analysis.

130 **BVOAC allows chemokinesis-mediated TEM into the tissue**

131 To quantify the number of neutrophils that left the vessel lumen and entered the matrix, we
132 used a 3D rendering and tracking approach to study chemokine-induced neutrophil TEM under
133 inflammatory conditions. This 3D rendering allowed us to observe a difference in number of
134 transmigration events that was not detectable using a 2D analysis (Figure 4A-B). Using this approach,
135 we accurately discriminated between adherent and transmigrated neutrophils (Figure 4A), revealing
136 a strong increase in both leukocyte TEM states in TNF-α-stimulated vessels compared to control
137 vessels (Figure 4C). Interestingly, neutrophils that crossed TNF-α-stimulated endothelium migrated

138 further away from the vessel than neutrophils that crossed untreated endothelium, indicating that
139 the inflamed endothelium may stimulate neutrophil migration (Figure 4D).
140 To test if neutrophils respond to a chemotactic gradient, we injected C5a, a chemoattractant,
141 into one of the matrix inlets (see schematic Figure 4E). Addition of C5a did not alter the number of
142 neutrophils that crossed inflamed endothelium (Figure 4H) but changed the migration direction of
143 neutrophils towards C5a significantly (Figure 4F-G, I). Interestingly, whereas the migration distance
144 that neutrophils travelled was not different between the two sides under control conditions (Figure
145 4J-left), in the presence of C5a on one side the migration distance towards this side was significantly
146 increased (Figure 4J-right). In summary, these data demonstrate that luminal application of TNF-α in
147 this BVOAC model strongly enhances neutrophil extravasation and entry into the surrounding matrix,
148 which can be directionally steered by applying a chemotactic gradient inside the matrix.

149 **T-cell transmigration through a HUVEC lined vessel and neutrophils transmigration in pancreatic**
150 **and lung microvascular vessels**

151 To examine the versatility of this system and determine whether this system is also suitable
152 for analysing T-cell TEM, we injected purified T-cells into the lumen of both inflamed and control
153 vessels. After 2.5 hours, vessels were flushed, fixed, and imaged (Figure 5A-B). We found that the
154 number of adhered and transmigrated T-cells was 5 times increased in inflamed vessels compared to
155 control conditions (Figure 5C). In addition, T-cells migrated further into the underlying matrix when
156 the vessels were inflamed (Figure 5D), in line with the finding that neutrophils also extended their
157 migration track when crossing inflamed endothelium. However, whereas neutrophils travelled from
158 the vessel into the matrix for on average 83 µm, T-cells only travelled on average 44 µm, indicating
159 that the intrinsic migration speed of neutrophils through the 3D matrix is 89% higher compared to T-
160 cells.
161 In addition to using different leukocyte subsets, we analysed if different endothelial cells may
162 be used to generate the vessel. For this, we used human microvascular endothelial cells from both
163 the lungs and pancreas . Both cell types formed a nice vessel (Figure 5E-F). Next, neutrophils were
164 added to the vessels of both endothelial cell types, similar to previous experiments. Neutrophils
165 transmigrated across both endothelial cell types and migrated into the matrix (Figure 5G). Although
166 the total number of cells in the field of view did not differ between lung and pancreas vessels (138
167 and 158 respectively), transmigration percentage was increases in the lung vessels (78% and 41%
168 respectively). The distance travelled by neutrophils from the vessel into the matrix was similar in
169 both cell types (Figure 5H). These data indicate that the BVOAC device is very versatile, both for
170 different leukocyte and endothelial cell types, and can be adjusted to the research question that
171 needs to be answered.

172 **Live cell imaging reveals differences in leukocyte migration**

173 We next investigated the source of the difference in migration distance between T-cells and
174 neutrophils. Although 3D confocal imaging analysis offers a more accurate detection of
175 transmigration events compared to 2D widefield imaging, it does not allow us to distinguish between
176 actual migration speed and relative track distance over time. Using high-speed imaging, we
177 generated Z-stacks of 200 µm with a time interval of 10 seconds, giving us sufficient spatiotemporal
178 resolution for semi-automatic tracking of individual leukocytes through the collagen matrix in time.
179 Automatic tracking was performed on all leukocytes in the field of view, after which tracks were
180 filtered to exclude neutrophils exiting or entering the field of view. For analysis requiring complete
181 leukocyte tracks, such as displacement or total track length, we selected 10 tracks per experiment
182 which were manually checked to assure quality of the data.

183 Using this approach, we were able to track migrating neutrophils or T-cells in time in 3
184 dimensions (Figure 6A-B and Supplemental Video 3-4). We found that the migration speed of T-cells
185 inside the matrix after crossing the inflamed endothelium is significantly slower on average than that
186 of neutrophils (Figure 6C; 0.10 µm/sec ± 0.03 and 0.20 µm/sec ± 0.02, respectively). Based on these
187 measurements neutrophil migration speed is 100% higher compared to T-cells, which is different
188 from the 89% larger migration distance observed in the endpoint experiment. To assess whether the
189 speed of both leukocyte subsets was consistent over time from the initial start until the end of the
190 recordings, we compared the initial and final migration speed, and found that both neutrophils and
191 T-cells maintain a constant speed over time (Figure 6D-E).

192 Next, we analysed the linearity of the migration tracks, which is defined as the ratio of the
193 displacement over the total distance travelled by that cell (Boissonnas *et al.*, 2007). This ratio has a
194 maximum of 1, which occurs when the cells travelled in a straight line from the start position to the
195 end position. We found that T-cells migrate in a more linear manner compared to neutrophils (Figure
196 6F; 0.25 ± 0.07 and 0.10 ± 0.02, respectively). Accordingly, the total distance travelled within the
197 same time frame was higher for neutrophils than for T-cells (Figure 6G; 948 µm vs. 400 µm,
198 respectively). These results indicated that neutrophils exerted a more intrinsic exploratory behaviour
199 than T-cells in our system. Therefore, we conclude that neutrophils migrate faster but wander
200 around more through the collagen, whereas T-cells migrate slower, but in a more directed fashion.

201 **C5a gradient increases neutrophil speed in the first half hour**

202 We examined to what extent the exploratory behaviour of neutrophils can be regulated by a
203 chemotactic gradient such as C5a. 3D live imaging of neutrophil migration in the presence of a C5a
204 gradient showed that most neutrophils migrated towards the chemoattractant (Figure 7A-B,

205 Supplemental Video 5), confirming our previous results. Interestingly, when analysing the direction of
206 migration over time, we observed that the C5a-driven migration pattern occurred predominantly in
207 the first 15 min of the experiment. After this timepoint, C5a-driven migration directionality was
208 strongly diminished and neutrophil migration directionality appeared to be random, as if no
209 chemoattractant was present (Figure 7C-D). We also calculated the speed of the neutrophils that
210 were exposed to C5a and found that over the course of the experiment, the speed was reduced
211 (Figure 7E). We found that the migration linearity was significantly increased in the presence of C5a
212 compared to control condition (Figure 7F; 0.17 ± 0.04 vs. 0.10 ± 0.02, respectively). The decreased
213 migration speed and increased directionality together lead to a total migration distance that was not
214 changed in the presence of C5a compared to control (Figure 7G). These data indicate that the
215 chemotactic gradient in the matrix disappeared in time, with the consequence that neutrophils
216 change their migratory behaviour from linear to random migration pattern.

217 In conclusion, this BVOAC device enables us to accurately visualize and analyse TEM of
218 primary human leukocytes in 3D over time, which can be modulated by applying a chemoattractant
219 gradient. As such, this novel platform holds great promise for future studies unravelling the complex
220 cellular and molecular mechanisms that underlie leukocyte TEM.

Discussion

Leukocyte extravasation through the vessel wall is mostly studied using classical *in vitro* 2D models that allow for analysis of the molecular details of this process. However, in these models, endothelial cells are typically cultured on artificial stiff substrates, which alters endothelial behaviour and responses. Moreover, these models preclude analysis of the final part of the leukocyte extravasation; penetration of the surrounding matrix. Thus, there is an urgent need for a proper *in vitro* model that mimics the *in vivo* conditions and allows for studying of molecular details of this process. We demonstrate that a hydrogel-based BVOAC model perfectly meets these demands and allows studying the full extravasation process at the single cell level in 3D over time.

In the human body, inflammation typically leads to leads to vasoconstriction by contracting smooth muscle cells around the vessel wall (Pleiner *et al.*, 2003; Lim and Park, 2014). Leukocyte extravasation mostly occurs in inflamed post-capillary venules, where the blood vessels only consist of a single layer of endothelial cells (Baluk *et al.*, 1998). Because inflammatory mediators such as TNF-α induce strong F-actin stress fibres, they are expected to induce cellular tension and potential contraction on an endothelial monolayer (Wójciak-Stothard *et al.*, 1998). In 2D monolayers, TNF-α stimulation leads to the formation of intracellular gaps, an observation which is supported by an increase in permeability. However, using the BVOAC model, we confirmed that TNF-α increased the number of F-actin stress fibres, and the vessel lumen diameter was reduced, instead of a loss of contact between individual endothelial cells and the formation of intracellular gaps. In addition, in the human body, vessels are surrounded by a collagen IV layer (Yurchenco, 2011; Xu and Shi, 2014). In our system, this collagen IV layer was also present, mimicking *in vivo*-like conditions. This indicated that the BVOAC much better represents the physiological situation than any 2D cell culture model used to study inflammation-related events.

In addition, when culturing endothelial cells on glass or plastics, F-actin stress fibres are prominently present through the cell body, even without inflammatory stimuli. In human arteries, these fibres are also prominently present, however, in veins and post-capillary venules such fibres are lacking (Van Geemen *et al.*, 2014). Under control conditions, the BVOAC model represents the *in vivo* non-inflamed condition, as we observed no endothelial F-actin stress fibres. Only upon stimulation with TNF-α stress fibres appear in the cell body. Therefore, we conclude that our *in vitro* generated vessels accurately represent both resting and inflamed states of blood vessels *in vivo*, and thus are a major improvement compared to conventional inflammatory 2D models.

Another point where the BVOAC system shows its potential as a model is importance of real-time analysis of migrating leukocytes in 3D. When comparing end point measurements with real-time TEM data, we found that our analysis of fixed samples leads to a large underestimation of the

255 migration distance, particularly for leukocytes such as neutrophils that exhibit a strong exploratory
256 behaviour. A schematic representation illustrating the various measurement methods and the
257 difference they report for identical events is displayed in Figure 8A. Based on end point
258 measurement, we observed that neutrophils migrated further away from the vessel than T-cells in
259 the same time frame, indicating higher migration speed for neutrophils. Using live imaging we found
260 that the effect is even larger than expected due to their exploratory behaviour through the matrix.
261 Live imaging also allowed us to discriminate between migration behaviour of the neutrophil away
262 from but also back towards the vessel. This type of migration behaviour would otherwise not be
263 observed.

264 T-lymphocyte migration is characterized by the stop and go manner they display to survey
265 the environment, which makes speed measurements challenging (Dupré *et al.*, 2015; Jerison and
266 Quake, 2020). Sadjadi and colleagues investigated the migration speed of T-cells in different collagen
267 concentrations (Sadjadi *et al.*, 2020). They tested 2, 4 and 5 mg/mL. In our system, we used
268 approximately 2,5 mg/mL and measured a speed of 6 µm/min, comparable with the speed observed
269 by Sadjadi et al. in 2 mg/mL collagen. This is supported by the study of Niggemann et al (1997), who
270 found a migration speed of 7 µm/min in a collagen concentration of 1.67 mg/mL (Niggemann *et al.*,
271 1997). *In vivo*, higher migration speeds are observed (10-15 µm/min) but this depends on activation
272 status and differs between organs (Miller *et al.*, 2002). Neutrophil migration speed measured in our
273 system is 12 µm/min. A recent study by Wolf et al. measured speed of neutrophils in 3.3 and 8
274 mg/mL collagen gels and observed migration speeds of 5-10 µm/min respectively (Wolf *et al.*, 2018).
275 Considering that the collagen concentration in our study is slightly lower, the speeds found in our
276 experiments support the speeds mentioned in literature for both T-cells and neutrophils.

277 The hydrogel-based BVOAC system allows us to study the full TEM process in time in great
278 detail, not hampered by the limitations of classical TEM models. However, there is an important
279 parameter of TEM lacking in this system, which is flow. The importance of flow for endothelial cell
280 function has been shown extensively and is known to affect TEM (Kitayama *et al.*, 2000; Conway *et*
281 *al.*, 2017; Polacheck *et al.*, 2017). The addition of flow to our BVOAC model would be the next
282 important step, allowing us to investigate the full TEM multistep process from rolling and adhesion,
283 to transmigration and penetration of the collagen matrix in one assay.

284 Using the BVOAC, we found that neutrophils migrate twice as fast compared to T-cells, and
285 both cell types showed increased migration distance in 3D when first crossing an inflamed
286 endothelial lining. This finding highlights the benefits and opportunities of a BVOAC model over 2D
287 models. Moreover, neutrophils migrate in a random fashion whereas T-cells have a much more
288 directed migration pattern. Under a chemotactic gradient the neutrophil migration adopts more T-
289 cell like directionality for a limited amount of time, before reverting to their exploratory migration

290 pattern. Schematic representations of the various migration dynamics are shown in Figure 8B.
291 Because of the real-time imaging possibility, we found that neutrophils can also migrate back to the
292 vessel once they have entered the matrix. Others have reported on this phenomenon, called reverse
293 transmigration, as well, using *in vivo* animal models (Woodfin *et al.*, 2011; Colom *et al.*, 2015). The
294 BVOAC model now opens new opportunities to study reverse transmigration at the molecular level.
295 This remarkable migration behaviour can also be found when neutrophils do not sense the
296 chemotactic gradient anymore, indicating that the endothelial vessel wall, might in fact attract
297 neutrophils back once the final destination in the tissue has been reached and gradients are cleared.
298 This type of migration is typical for resolving inflammation and was studied using *in vivo* models
299 (Peiseler and Kubes, 2018; Bogoslowski *et al.*, 2020). In this situation the BVOAC model may offer
300 new opportunities to study this migration behaviour as well.

301 In conclusion, TEM experiments with the BVOAC platform enable the exploration of many
302 parameters previously unobtainable. The level of imaging and analysis determines which aspects of
303 the leukocyte extravasation can be observed. Our comparison between 2D, 3D and live 3D imaging of
304 leukocyte TEM dynamics demonstrates that it is imperative to image and analyse TEM experiments
305 in 3D over time for an accurate interpretation of the events in this system. This hydrogel-based
306 BVOAC model now facilitates studying the full process of human leukocyte extravasation under
307 inflammatory conditions *in vitro* and thereby identify the underlying cellular characteristics and
308 molecular requirements.

309 ## Material and methods

310 Cell culture and seeding

311 Pooled Human Umbilical Vein Endothelial Cells (HUVEC, Lonza P1052, #C2519A) were cultured at
312 37˚C with 5% CO_2 on fibronectin-coated culture flasks in Endothelial Cell Growth Medium 2 (EGM-2,
313 Promocell #C22011) supplemented with supplement Mix (Promocell, #C39216). HUVECs were
314 passaged at 60-70% confluency and used for experiments between passage 3-7. Pulmonary
315 (HPaMVC, Pelobiotech, # PB-CH-147-4011) and lung (HPuMVC, Lonza, #CC-2527) microvascular cells
316 were cultured at 37˚C with 5% CO_2 on fibronectin-coated culture flasks in SupplementPack
317 Endothelial Cell GM2 containing 0.01 mL/mL L-Glutamine (Sigma, #G3202), 0.02 mL/mL Fetal calf
318 serum (FCS, C-37320), 5 ng/mL human epidermal growth factor (hEGF, C-30224), 0.2 µg/ml
319 Hydrocortisone (HC, C-31063), 0.5 ng/mL Vascular endothelial growth factor 165 (VEGF, C-3260), 10
320 ng/mL human basic Fibroblast Growth Factor (hbFGF, C-30321), 20 ng/mL Insulin-like Growth Factor
321 (R3, C-31700), 1 µg/mL Ascorbic Acid (AA, C-31750). The cells were passaged at 60-70% confluency
322 and used for experiments between passage 5-8.

323 Collagen gel preparations

324 All following steps were carried out on ice to halt polymerization of the collagen. 50 µl of 10x PBS
325 (Gibco, #70011-044) was added carefully on top of 250 µl of bovine collagen type-1 (10 mg/mL
326 FibriCol, Advanced BioMatrix, #5133) and mixed. When the solution was sufficiently mixed, 48.6 µl of
327 0.1 M NaOH was added and the mixture was put on ice for 10 minutes. pH was checked before
328 mixing 1:1 with cell culture medium, bringing the final collagen concentration to 2,5 mg/mL.

329 3D vessel production

330 The LumeNext devices were obtained from the Beebe Lab. For more information about this system,
331 please contact David Beebe. The hollow chambers were coated with 1% Polyethylenimine (PEI,
332 Polysciences, #23966) and incubated for 10 min at room temperature (RT), sequentially chambers
333 were coated with 0.1% glutaraldehyde (Merck, #104239) and washed 5x with Water for Injection
334 (WFI, Gibco, #A12873-01). Chambers were airdried before adding of collagen. Collagen was prepared
335 according to the protocol above. 5 µL collagen was added to the chambers and allowed to
336 polymerize for 30 min. The chamber is about $2mm^3$ in total. PBS drenched cotton balls were added to
337 the device to prevent drying in of the collagen. When polymerization of collagen was confirmed, rods
338 were removed and medium was added to the lumen. HUVECs were dissociated using Trypsin/EDTA
339 (Sigma, #T4049), neutralized 1:1 with Trypsin Neutralising Solution (TNS, Lonza, #CC-5002), spun
340 down and concentrated to $15*10^6$ cells/mL in EGM-2. 5 µl of cell suspension was added per vessel

341 and the devices were placed in a head-over-head rotator for 2 hours at 1 RPM at 37˚C with 5% CO_2
342 for seeding. Medium was replaced twice daily and vessels were allowed to mature for 2 days before
343 use.

344 Neutrophil and T-cell isolation

345 Polymorphonuclear neutrophils (PMN) were isolated from whole blood derived from healthy donors
346 who signed an informed consent under the rules and legislation in place within the Netherlands and
347 maintained by the Sanquin Medical Ethical Committee. Heparinised whole blood was diluted (1:1)
348 with 10% (v/v) trisodium citrate diluted in PBS. Diluted whole blood was pipetted carefully on 12.5
349 mL Percoll (RT) 1.076 g/mL. Tubes were centrifuged (Rotanta 96R) at 450 g, slow start, low brake for
350 20 min. Plasma and peripheral blood mononuclear cell (PBMC) ring fraction were removed.
351 Erythrocytes were lysed in an ice-cold isotonic lysis buffer (155 mM NH4CL, 10 mM KHCO3, 0.1 mM
352 EDTA, pH7.4 in WFI) for 10 min. Neutrophils were pelleted at 450 g for 5 min at 4°C, resuspended in
353 lysis buffer and incubated for 5 min on ice. Neutrophils were centrifuged again at 450 g for 5 min at
354 4°C, washed once with PBS, centrifuged again at 450 g for 5 min at 4°C and resuspended in HEPES
355 medium (20 mM HEPES, 132 mM NaCl, 6 mM KCL, 1 mM CaCL2, 1 mM MgSO4, 1.2 mM K2HPO4, 5
356 mM glucose, Sigma-Aldrich, and 0.4% (w/v) human serum albumin, Sanquin Reagents), pH 7.4) and
357 kept at room temperature for no longer than 4 h until use. This isolation method typically yields
358 >95% purity.

359 Cytotoxic T lymphocytes (CTL) were isolated from density-gradient isolated PBMC by use of magnetic
360 separation. Whole blood was diluted 1:1 with balanced salt solution at RT and layered onto Ficoll
361 Paque PLUS (GE Healthcare, #GE17-1440-02) followed by centrifugation at 400 g for 30 min. From
362 here on cells and buffers are kept at 4°C. The PBMC ring fraction was harvested and washed three
363 times using isolation buffer (PBS + 0.5% FCS). CTL were isolated negatively using the Miltenyi CD8 T-
364 cell isolation kit (Miltenyi, #130-096-495) with LS columns (Miltenyi, #130-042-401) and a
365 QuadroMACS according to the manufacturer's instruction. Afterwards CTL were harvested and
366 resuspended in RPMI 1640 (Thermo Fisher, #61870010) containing 10% FBS and kept at 37°C and 5%
367 CO2 overnight until use. T-cell purity is typically >95-98% $CD8^+$ T cells.

368 Immunofluorescent staining

369 The vessel lumen was washed 3 times with PBS ++ (PBS with 1mM CaCl2, 0.5mM MgCl2) and fixed
370 with 4% paraformaldehyde (PFA, Merck, #30525-89-4) at 37°C for 15 min. Afterwards vessels were
371 incubated with directly conjugated antibodies in PBST (PBS with 0.2% BSA and 0.1% Tween) O/N at
372 4°C. After staining vessels were washed 3 times with PBS and kept at 4°C awaiting imaging. The
373 following antibodies and stains were used: Mouse anti-hVE-cadherin/CD144 AF647 conjugated ([55-

374 7H1], BD, #561567), Phalloidin AF488 conjugated (Molecular Probes, #A12379), Hoechst 33342
375 (Molecular probes, #H-1399), Mouse anti-hICAM-1 AF546 conjugated (15.2, Santa Cruz, #sc-
376 107AF546), anti-Collagen IV (Abcam, #ab6586).

377 FITC-dextran leakage assay

378 6 µL of 70 kDa FITC-dextran in EGM-2 (5 mg/mL, Merck, #46945) was added to each vessel. Thrombin
379 (1U/mL, Merck, #T1063) was added to the dextran and injected at the same time. The device was
380 placed under a widefield microscope and every 10 s an image was captured. Images were analysed in
381 Fiji (ImageJ, version 1.52). Fluorescent intensity was measured over the cross-section of the vessel at
382 6 timepoints throughout the movie.

383 TEM assay

384 Endothelial cells were stained with CellTracker™ Green CMFDA Dye (1 µM, Molecular Probes,
385 #C7025) according to manufactures protocol, before seeding. TNF-α (10 ng/mL, Peprotech, #300-
386 01A) was added O/N inside the vessel. Leukocytes were stained with Vybrant™ DiD Cell-Labelling
387 Solution (1 µM, Molecular Probes) for 15 min at 37°C, pelleted at 450 g for 5 minutes, washed,
388 pelleted again and resuspended in medium. 2 µl of $16*10^6$ neutrophils or T-cells per mL were added
389 per vessel. For live imaging migration was imaged for 60 min and for endpoint conditions neutrophils
390 were allowed to migrate for 2.5 hours at 37°C. Vessels were flushed with PBS++ and fixed for 15 min
391 with 4% PFA. Vessels were stored in PBS at 4°C until imaging.

392 Imaging and analysis

393 Brightfield images were acquired on an Axio Observer Microscope (ZEISS) using Zen 2 blue edition
394 using a 10x air objective (ZEISS, #420341-9911, Plan-Neofluor 10x/0.3 Ph1). Fluorescent staining of
395 the vessels was imaged using a SP8 confocal microscope (Leica) with a 25x long working distance
396 water objective (Leica, #15506375, HC FLUOTAR L 25x/0.95). Control and inflamed vessels were
397 imaged using identical settings. TEM experiments (both live and fixed) were imaged on an LSM980
398 Airyscan2 (ZEISS) with a 10x air objective (ZEISS, #420640-9900-000, Objective Plan-Apochromat
399 10x/0.45). Laser power was kept to a minimum to limit phototoxicity during live imaging. The
400 transmigration assays and the 3D rendering/orthogonal views were analysed with IMARIS Bitplane
401 software (Version 9.5/9.6) while the leakage data, zoom-in on the cell junctions and collagen IV stain
402 were analysed with Fiji (ImageJ, version 1.52).

403 3D analysis in Imaris

To analyse the distance from the neutrophils to the surface of the vessel, the spot function was applied to automaticallydetect fluorescently labelled neutrophils and a surface rendering of the vessel was generated from the XYZ-fluorescent label. The vessel surface was created manually by tracing the outline of the vessel, the software then rendered a cylindrical shape corresponding to the immunofluorescent signal. Possible holes were automatically filled by the software. The spot function was applied automatically with the same parameters for all experiments, but checked manually afterwards to ensure detection was correct. When both the vessel surface and spots were created, data like number of neutrophils and distance to the vessels could be extracted from the IMARIS spot function and further analysed in excel.

Statistics

Statistics were performed in GraphPad Prism 9 (version 9.0.1). Data was checked for normality via the Anderson-Darling test. If normally distributed a (paired) students' t-test was used to test for statistical significance. Statistical significance is indicated as follows: *= $p<0.05$, **= $p<0.01$, ***= $p<0.001$, ****= $p<0.0001$.

Acknowledgements

This work was supported by LSBR grant # 1649 (A.C.I.v.S.), LSBR grant # 1820 (L.K.), NIH R01AI134749 (D.J.B.), NIH R33CA225281 (D.J.B.), NIH P30CA014520 (D.J.B.) and ZonMW NWO Vici grant #91819632 (J.D.v.B.). D.J.B. holds equity in Bellbrook Labs LLC, Tasso Inc., Salus Discovery LLC, Lynx Biosciences Inc., Stacks to the Future LLC, Turba LLC, Flambeau Diagnostics LLC, and Onexio Biosystems LLC. D.J.B. is also a consultant for Abbott Laboratories.

Author contributions

A.C.I.v.S., L.K. and R.S. performed experiments. M.B., A.C.I.v.S. and L.K. analysed data. M.J.B. advised and provided essential chips. A.C.I.v.S., L.K., J.D.v.B. and M.A.N. wrote manuscript. J.D.v.B. and M.A.N. supervised the study.

References

428 Ando, K. *et al.* (2013) 'Rap1 potentiates endothelial cell junctions by spatially controlling myosin I activity and
429 actin organization', *Journal of Cell Biology*. J Cell Biol, 202(6), pp. 901–916. doi: 10.1083/jcb.201301115.

430 Baluk, P. *et al.* (1998) 'Endothelial gaps and adherent leukocytes in allergen-induced early- and late-phase
431 plasma leakage in rat airways', *American Journal of Pathology*. American Society for Investigative Pathology,
432 152(6), pp. 1463–1476. Available at: /pmc/articles/PMC1858452/?report=abstract (Accessed: 25 February
433 2021).

434 Bogoslowski, A. *et al.* (2020) 'Neutrophils Recirculate through Lymph Nodes to Survey Tissues for Pathogens',
435 *The Journal of Immunology*. The American Association of Immunologists, 204(9), p. ji2000022. doi:
436 10.4049/jimmunol.2000022.

437 Boissonnas, A. *et al.* (2007) 'In vivo imaging of cytotoxic T cell infiltration and elimination of a solid tumor',
438 *Journal of Experimental Medicine*, 204(2), pp. 345–356. doi: 10.1084/jem.20061890.

439 Colom, B. *et al.* (2015) 'Leukotriene B4-Neutrophil Elastase Axis Drives Neutrophil Reverse Transendothelial Cell
440 Migration InVivo', *Immunity*. Cell Press, 42(6), pp. 1075–1086. doi: 10.1016/j.immuni.2015.05.010.

441 Conway, D. E. *et al.* (2017) 'VE-Cadherin Phosphorylation Regulates Endothelial Fluid Shear Stress Responses
442 through the Polarity Protein LGN', *Current Biology*. Cell Press, 27(14), pp. 2219-2225.e5. doi:
443 10.1016/j.cub.2017.06.020.

444 Dupré, L. *et al.* (2015) 'T lymphocyte migration: An action movie starring the actin and associated actors',
445 *Frontiers in Immunology*, 6(NOV). doi: 10.3389/fimmu.2015.00586.

446 Farahat, W. A. *et al.* (2012) 'Ensemble Analysis of Angiogenic Growth in Three-Dimensional Microfluidic Cell
447 Cultures', *PLoS ONE*. Edited by C. Egles. Public Library of Science, 7(5), p. e37333. doi:
448 10.1371/journal.pone.0037333.

449 Van Geemen, D. *et al.* (2014) 'F-actin-anchored focal adhesions distinguish endothelial phenotypes of human
450 arteries and veins', *Arteriosclerosis, Thrombosis, and Vascular Biology*, 34(9), pp. 2059–2067. doi:
451 10.1161/ATVBAHA.114.304180.

452 Grönloh, M. L. B., Arts, J. J. G. and van Buul, J. D. (2021) 'Neutrophil transendothelial migration hotspots –
453 mechanisms and implications', *Journal of Cell Science*, 134(7). doi: 10.1242/jcs.255653.

454 Heller, R. A. and Krönke, M. (1994) 'Tumor necrosis factor receptor-mediated signaling pathways', *Journal of*
455 *Cell Biology*. J Cell Biol, pp. 5–9. doi: 10.1083/jcb.126.1.5.

456 Huynh, J. *et al.* (2011) 'Age-related intimal stiffening enhances endothelial permeability and leukocyte
457 transmigration', *Science Translational Medicine*. Sci Transl Med, 3(112). doi: 10.1126/scitranslmed.3002761.

458 Jerison, E. R. and Quake, S. R. (2020) 'Heterogeneous T cell motility behaviors emerge from a coupling between
459 speed and turning in vivo', *eLife*, 9, pp. 1–26. doi: 10.7554/eLife.53933.

460 Jiménez-Torres, J. A. *et al.* (2016) 'LumeNEXT: A Practical Method to Pattern Luminal Structures in ECM Gels',
461 *Advanced Healthcare Materials*. Wiley-VCH Verlag, 5(2), pp. 198–204. doi: 10.1002/adhm.201500608.

462 Kim, S. *et al.* (2016) 'Interstitial flow regulates the angiogenic response and phenotype of endothelial cells in a
463 3D culture model', *Lab on a Chip*. Royal Society of Chemistry, 16(21), pp. 4189–4199. doi: 10.1039/c6lc00910g.

464 Kitayama, J. *et al.* (2000) 'Shear Stress Affects Migration Behavior of Polymorphonuclear Cells Arrested on
465 Endothelium', *Cellular Immunology*, 203(1), pp. 39–46. doi: https://doi.org/10.1006/cimm.2000.1671.

466 Lim, S. and Park, S. (2014) 'Role of vascular smooth muscle cell in the inflammation of atherosclerosis', *BMB*
467 *Reports*, 47(1), pp. 1–7. doi: 10.5483/BMBRep.2014.47.1.285.

468 Miller, M. J. *et al.* (2002) 'Two-photon imaging of lymphocyte motility and antigen response in intact lymph
469 node', *Science*, 296(5574), pp. 1869–1873. doi: 10.1126/science.1070051.

470 Muller, W. A. and Luscinskas, F. W. (2008) 'Chapter 9 Assays of Transendothelial Migration In Vitro', *Methods in*

Enzymology. NIH Public Access, pp. 155–176. doi: 10.1016/S0076-6879(08)02009-0.

Van Nieuw Amerongen, G. P. *et al.* (1998) 'Transient and prolonged increase in endothelial permeability induced by histamine and thrombin: Role of protein kinases, calcium, and RhoA', *Circulation Research*. Lippincott Williams and Wilkins, 83(11), pp. 1115–1123. doi: 10.1161/01.res.83.11.1115.

Niggemann, B. *et al.* (1997) 'Locomotory phenotypes of human tumor cell lines and T lymphocytes in a three-dimensional collagen lattice', *Cancer Letters*, 118(2), pp. 173–180. doi: 10.1016/S0304-3835(97)00328-5.

Peiseler, M. and Kubes, P. (2018) 'Macrophages play an essential role in trauma-induced sterile inflammation and tissue repair', *European Journal of Trauma and Emergency Surgery*. Springer Berlin Heidelberg, pp. 335–349. doi: 10.1007/s00068-018-0956-1.

Pleiner, J. *et al.* (2003) 'Inflammation-Induced Vasoconstrictor Hyporeactivity Is Caused by Oxidative Stress', *Journal of the American College of Cardiology*. Elsevier Masson SAS, 42(9), pp. 1656–1662. doi: 10.1016/j.jacc.2003.06.002.

Polacheck, W. J. *et al.* (2017) 'A non-canonical Notch complex regulates adherens junctions and vascular barrier function', *Nature*, 552(7684), pp. 258–262. doi: 10.1038/nature24998.A.

Sadjadi, Z. *et al.* (2020) 'Migration of Cytotoxic T Lymphocytes in 3D Collagen Matrices', *Biophysical Journal*. Biophysical Society, 119(11), pp. 2141–2152. doi: 10.1016/j.bpj.2020.10.020.

Sobrino, A. *et al.* (2016) '3D microtumors in vitro supported by perfused vascular networks', *Scientific Reports*. Nature Publishing Group, 6(1), pp. 1–11. doi: 10.1038/srep31589.

Stroka, K. M. and Aranda-Espinoza, H. (2011) 'Endothelial cell substrate stiffness influences neutrophil transmigration via myosin light chain kinase-dependent cell contraction', *Blood*. The American Society of Hematology, 118(6), pp. 1632–1640. doi: 10.1182/blood-2010-11-321125.

Virumbrales-Muñoz, M. *et al.* (2020) 'Microfluidic lumen-based systems for advancing tubular organ modeling', *Chemical Society Reviews*. Royal Society of Chemistry, pp. 6402–6442. doi: 10.1039/d0cs00705f.

Wójciak-Stothard, B. *et al.* (1998) 'Regulation of TNF-α-induced reorganization of the actin cytoskeleton and cell-cell junctions by Rho, Rac, and Cdc42 in human endothelial cells', *Journal of Cellular Physiology*. John Wiley & Sons, Ltd, 176(1), pp. 150–165. doi: 10.1002/(SICI)1097-4652(199807)176:1<150::AID-JCP17>3.0.CO;2-B.

Wolf, K. *et al.* (2018) 'Nucleus despite Incomplete Segmentation of the Inflammation Exhibit Efficient Migration Immature Neutrophils Released in Acute'. doi: 10.4049/jimmunol.1801255.

Wong, K. H. K. *et al.* (2012) 'Microfluidic models of vascular functions', *Annual Review of Biomedical Engineering*. Annu Rev Biomed Eng, pp. 205–230. doi: 10.1146/annurev-bioeng-071811-150052.

Woodfin, A. *et al.* (2011) 'The junctional adhesion molecule JAM-C regulates polarized transendothelial migration of neutrophils in vivo', *Nature Immunology*. Nat Immunol, 12(8), pp. 761–769. doi: 10.1038/ni.2062.

Woodfin, A., Voisin, M. B. and Nourshargh, S. (2010) 'Recent developments and complexities in neutrophil transmigration', *Current Opinion in Hematology*. Curr Opin Hematol, pp. 9–17. doi: 10.1097/MOH.0b013e3283333930.

Xu, J. and Shi, G.-P. (2014) 'Vascular wall extracellular matrix proteins and vascular diseases', *Biochimica et Biophysica Acta*, 1842(11), pp. 2106–2119. doi: 10.1016/j.bbadis.2014.07.008.Vascular.

Yamada, K. M. and Sixt, M. (2019) 'Mechanisms of 3D cell migration', *Nature Reviews Molecular Cell Biology*. Nature Research, pp. 738–752. doi: 10.1038/s41580-019-0172-9.

Yurchenco, P. D. (2011) 'Basement membranes: Cell scaffoldings and signaling platforms', *Cold Spring Harbor Perspectives in Biology*, 3(2), pp. 1–27. doi: 10.1101/cshperspect.a004911.

Zervantonakis, I. K. *et al.* (2012) 'Three-dimensional microfluidic model for tumor cell intravasation and endothelial barrier function', *Proceedings of the National Academy of Sciences of the United States of America*. National Academy of Sciences, 109(34), pp. 13515–13520. doi: 10.1073/pnas.1210182109.

Zheng, Y. *et al.* (2012) 'In vitro microvessels for the study of angiogenesis and thrombosis', *Proceedings of the National Academy of Sciences of the United States of America*. National Academy of Sciences, 109(24), pp. 9342–9347. doi: 10.1073/pnas.1201240109.

Figure Legends

Figure 1. Making and characterization of the BVOAC. Overview of the device (A) containing six chambers to make a BVOAC, zoom-in on one BVOAC and schematic overview of one vessel place. DIC (B) and confocal (C) image of a lumen lined with endothelial cells (D) and orthogonal view showing the open lumen of the BVOAC and the Imaris surface rendering. Zoom in on the BVOAC in D showing the endothelial monolayer (E). Representative images of leakage of 70 kDa dextran in the BVOAC (F) and quantification of the leakage 5 min after injection (G). Quantification was done by measuring the average fluorescent intensity over the Y axis of the image which is then normalised to the maximum signal measured. The red dotted lines represent the vessel outlines. Scalebar = 3 mm + 1 mm (A), 100 µm (B, C, D), 50 µm (E).

Figure 2. TNF-α in the vessel induces inflammation. Overview of a control (A) or TNF-α treated vessels (B). Quantification of the number of cells (C) and vessels diameter (D) in TNF-α treated vessels compared to control vessels. Representative images of control and inflamed endothelial cells (E) and junctions with line plots showing the localization of VE-cadherin and actin in these junctions (F). Representative image of the presence of Collagen IV around the vessels (G). Orthogonal view of a vessel with collagen IV staining around (H). Scalebar = 100 µm (A, B), 50 µm (E, H), 25 µm (F, G). Data quantified from 5 (Ctrl), 9 (TNF-α) BVOAC for the number of ECs per BVOAC, diameter 10 (Ctrl) and 20 (TNF-α) BVOAC, staining's and line plots 3 BVOAC per condition.

Figure 3.Vessel and leukocyte analysis in Imaris. Microscopy image depicting the BVOAC (green) with the neutrophils (white) from top (A) and side view (B). Surface of the BVOAC (C) and the leukocytes (D). Overview of the BVOAC surface with colour coded spots based on the distance from surface allowing calculations and analysis (E). Distribution of the distance between the leukocytes and the vessel displayed in E (F). Schematic overview of the different transmigration steps: adhering to the endothelial cells on the inside of the lumen (Blue circle), diapedeses (Pink circle) and transmigrated cells (Red circle) (G). Orthogonal view of stills taken from detailed high-speed imaging of neutrophil TEM in the vessel over time (H). Scalebar = 150 µm (B-D), 100µm (A,E), 15 µm (H).

Figure 4. Neutrophil transmigration in a 3D environment. Representative top view (A) and side view (B) images of neutrophil transmigration in control and TNF-α treated BVOAC. Quantification of the number of neutrophils per field of view (C) and average transmigration distance after exiting the BVOAC (D). Diagram of the experiment with one-sided addition of C5a (E). Representative top view (F) and side view (G) images of neutrophil transmigration in TNF-α treated BVOAC with C5a or PBs on one side. Quantification of the total number of transmigrated neutrophils per field of view (H), # of neutrophils per side of PBS and C5a treated BVOAC (I) and average migration distance between left and right of PBS or C5a treated BVOAC (J). Scalebar = 150 µm. Data quantified from 4 BVOAC per condition for neutrophil TEM and 3 BVOAC per condition for C5a TEM.

552 **Figure 5. T-cell transmigration in a 3D-environment.** Representative top view (A) and side view (B) images of T-
553 cell transmigration in control and TNF-α treated BVOAC. Quantification of number of transmigrated cells (C)
554 and cumulative transmigration distance (D). Representative top view (E) and side view (F) images of neutrophil
555 transmigration in vessels lined with lung or pancreatic endothelial cells. Quantification of number of adhered
556 and transmigrated cells (G) and migration distance of the transmigrated cells (H). Scalebar = 50 µm. Data
557 quantified from 4 (pancreas), 5 (Ctrl, lung vessels) and 6 (TNF-α) vessels per condition.

558 **Figure 6. Live transmigration of neutrophils and T-cells.** (A) Stills from a video in which neutrophils and T-cells
559 migrate out of the BVOAC. Per condition one track representing the general migration manner of that
560 leukocyte is highlighted. (B) Zoom-in on the track at T=60 of both neutrophils and T-cells. Quantification of the
561 average track speed (C), initial and final migration speed of neutrophils (D) and T-cells (E), linearity (F), track
562 length (G) for both neutrophils and T-cells. Scalebar = 50 µm. Data quantified from 10 cells per BVOAC and 3
563 BVOAC per condition.

564 **Figure 7. Live transmigration of neutrophils and migration dynamics with C5a.** Stills from a movie showing the
565 migration of neutrophils towards one side with a side (A) and top (B) view. Quantification of the direction of
566 the neutrophils in control and the C5a condition over time (C, D). This windrose plot shows the distribution of
567 leukocyte migration directions at distinct times as shown in the legend. Each concentric axe indicates 1.7% of
568 the total number of neutrophil movements at the indicated time. The red line represents the situation where
569 leukocyte migration in every direction is equal, and directionality is not observed. Quantification of the initial
570 and final speed of neutrophils in the presence of C5a (E), endpoint distance from the vessel (F) and the ratio
571 between the end point distance from the vessel and the total length travelled, also called linearity (G). Scalebar
572 = 50 µm. Data quantified from 10 cells per BVOAC and 3 BVOAC per condition.

573 **Figure 8. Different imaging methods to study different aspects of leukocyte (trans)migration.** (A) Schematic
574 representation of the similar experiment imaged in 2D, 3D or live 3D and with leukocytes perceived to be
575 outside of the vessel indicated as green dots. 2D imaging underestimates the number of extravasated
576 leukocytes because cells underneath the vessel are indistinguishable from cells inside the BVOAC. 3D live
577 imaging allows the tracking of cells over time and therefore analysis of migration dynamics which is not
578 possible based on 3D endpoint imaging. (B) Migration dynamics of different leukocytes in a 3D matrix. T-cells
579 migrate slower and more linear, while neutrophils travel faster while wandering around. When adding a
580 chemoattractant to neutrophils, they initially migrate at a similar speed compared to control, but much more
581 linear. Over time however they lose speed and directionality. Red = slower migration, green = faster migration.

Figure 1

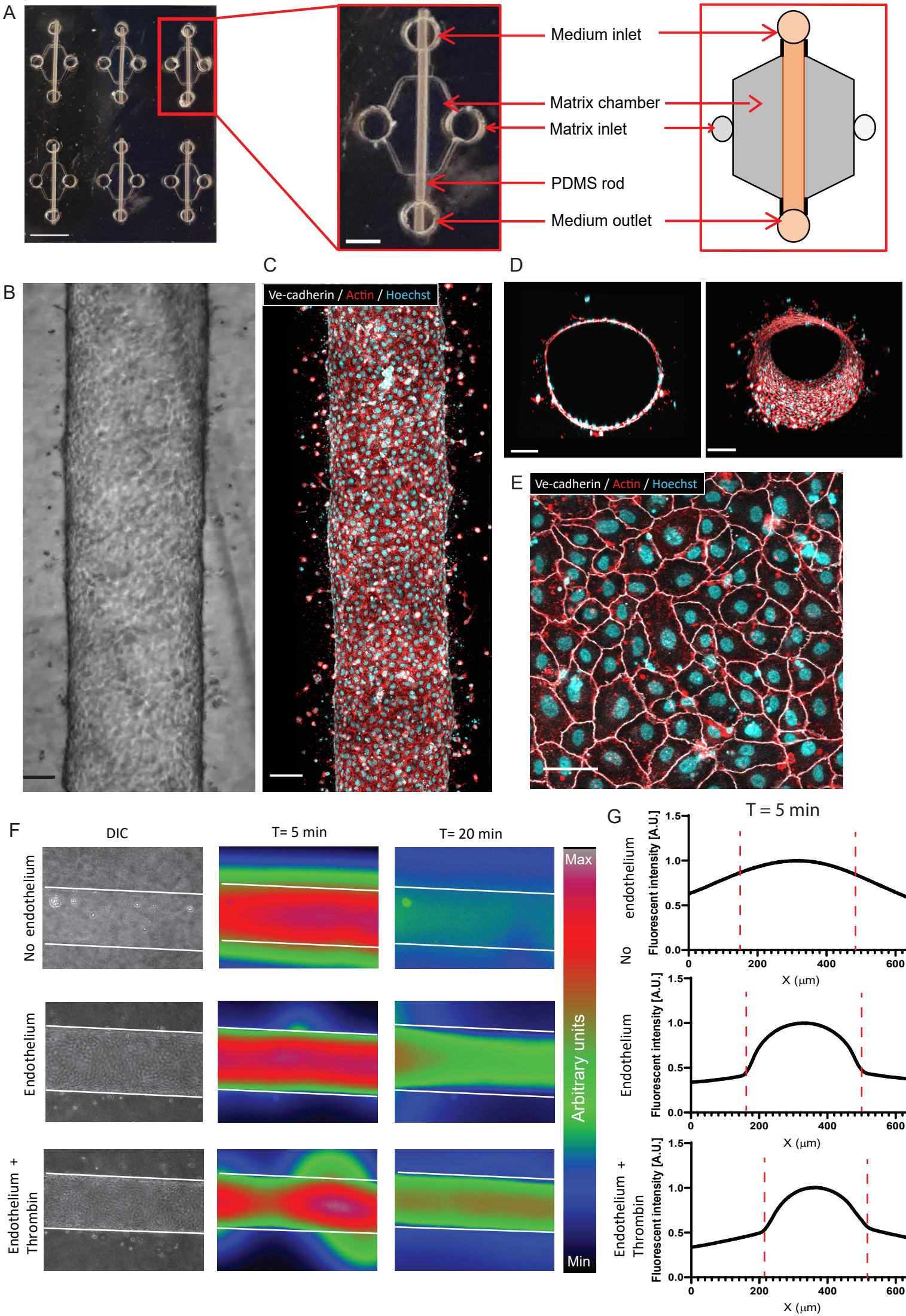
A
Medium inlet
Matrix chamber
Matrix inlet
PDMS rod
Medium outlet
B
C
Ve-cadherin / Actin / Hoechst
D
E
Ve-cadherin / Actin / Hoechst
F
DIC
T= 5 min
T= 20 min
No endothelium
Endothelium
Endothelium + Thrombin
Max
Arbitrary units
Min
G
T = 5 min
Fluorescent intensity [A.U.]
X (µm)
No endothelium
Endothelium
Endothelium + Thrombin
0.0
0.5
1.0
1.5
0
200
400
600

Figure 2

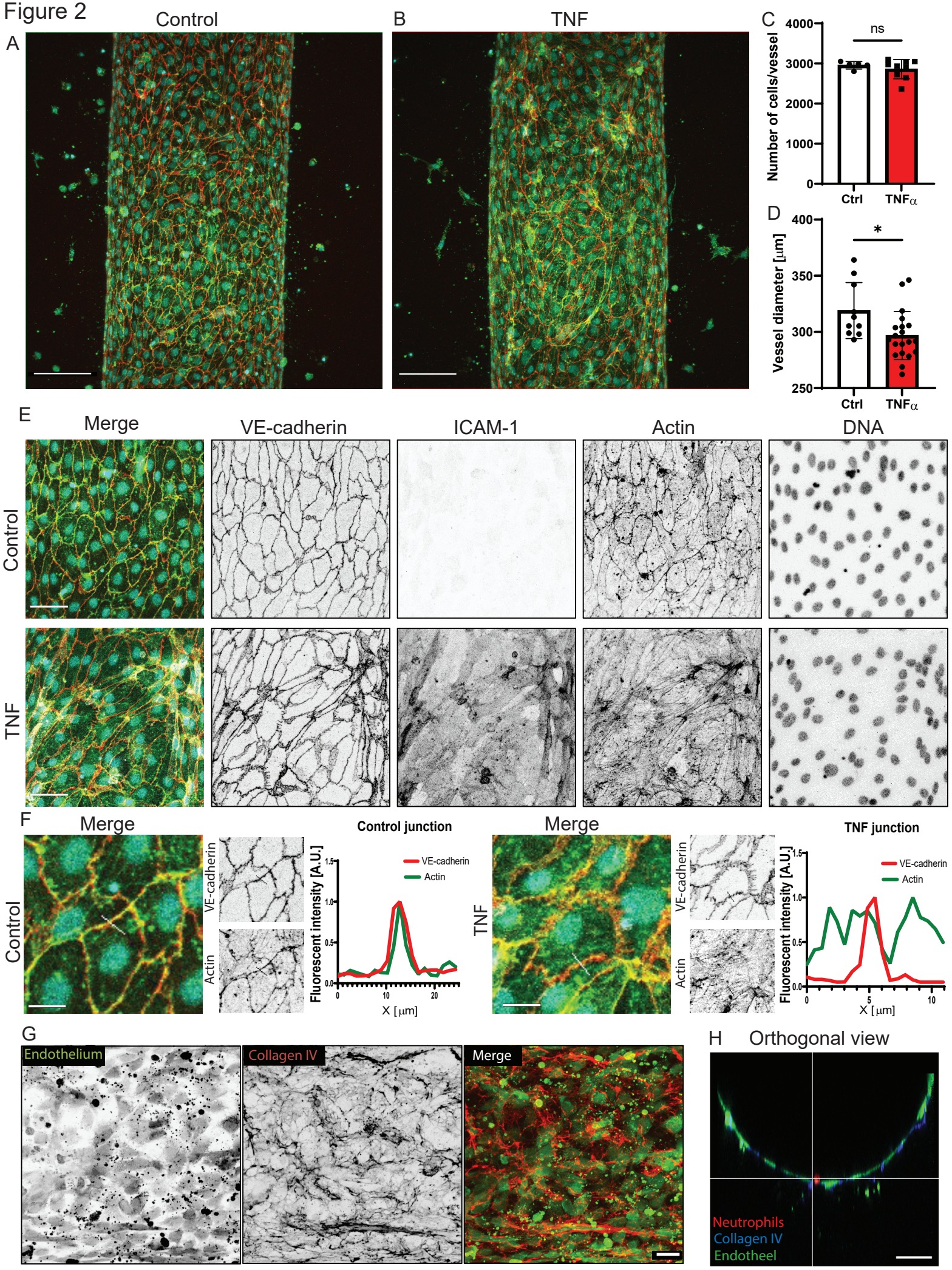
A
Control
B
TNF
C
Number of cells/vessel
4000
3000
2000
1000
0
ns
Ctrl
TNFα
D
Vessel diameter [µm]
400
350
300
250
*
Ctrl
TNFα
E
Merge
VE-cadherin
ICAM-1
Actin
DNA
Control
TNF
F
Merge
Control junction
VE-cadherin
Actin
Fluorescent intensity [A.U.]
X [µm]
Merge
TNF junction
VE-cadherin
Actin
Fluorescent intensity [A.U.]
X [µm]
G
Endothelium
Collagen IV
Merge
H
Orthogonal view
Neutrophils
Collagen IV
Endotheel

Figure 3

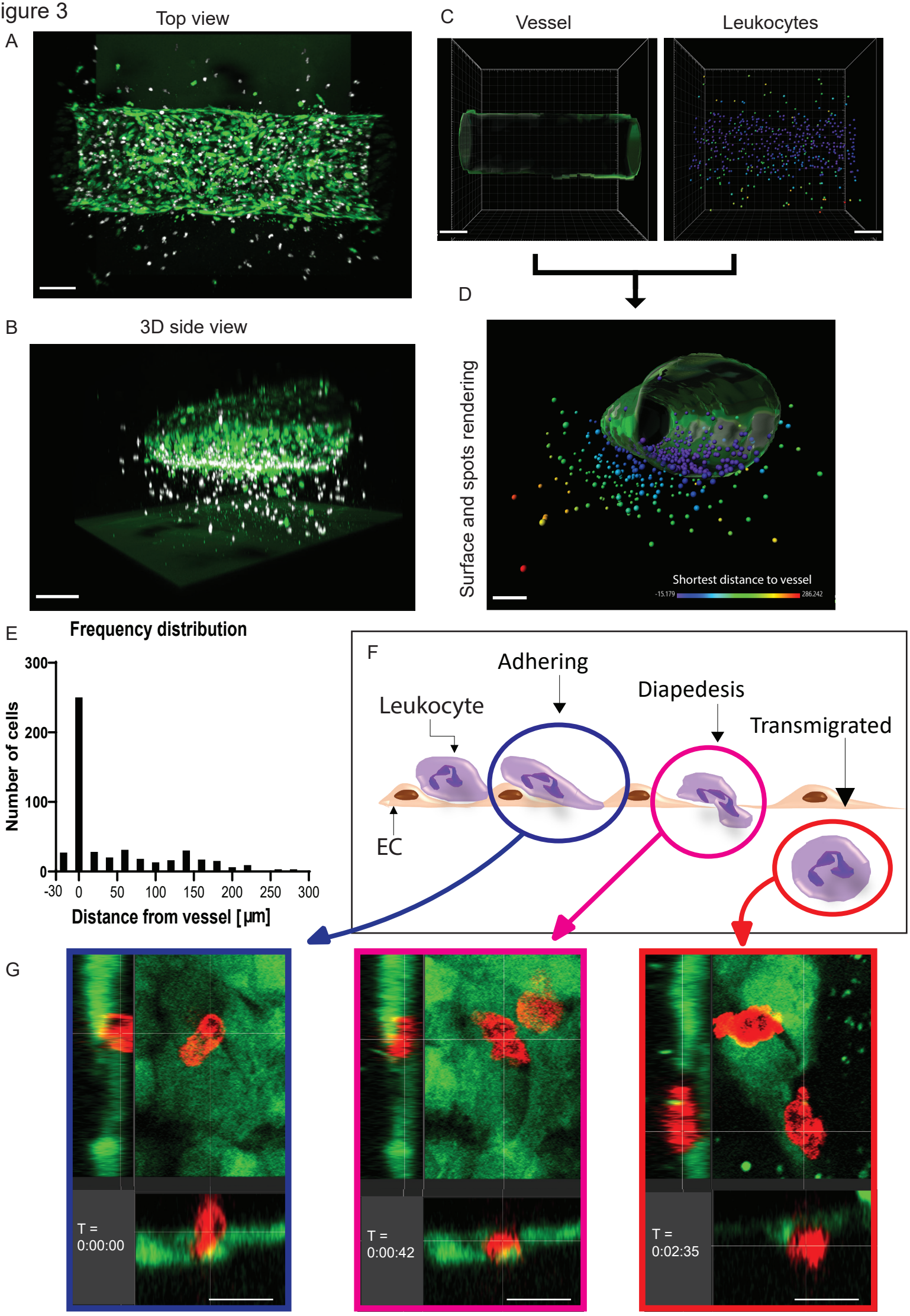
A
Top view
B
3D side view
C
Vessel
Leukocytes
D
Surface and spots rendering
Shortest distance to vessel
-15.179
286.242
E
Frequency distribution
Number of cells
300
200
100
0
-30
0
50
100
150
200
250
300
Distance from vessel [µm]
F
Adhering
Leukocyte
Diapedesis
Transmigrated
EC
G
T =
0:00:00
T =
0:00:42
T =
0:02:35

Figure 4

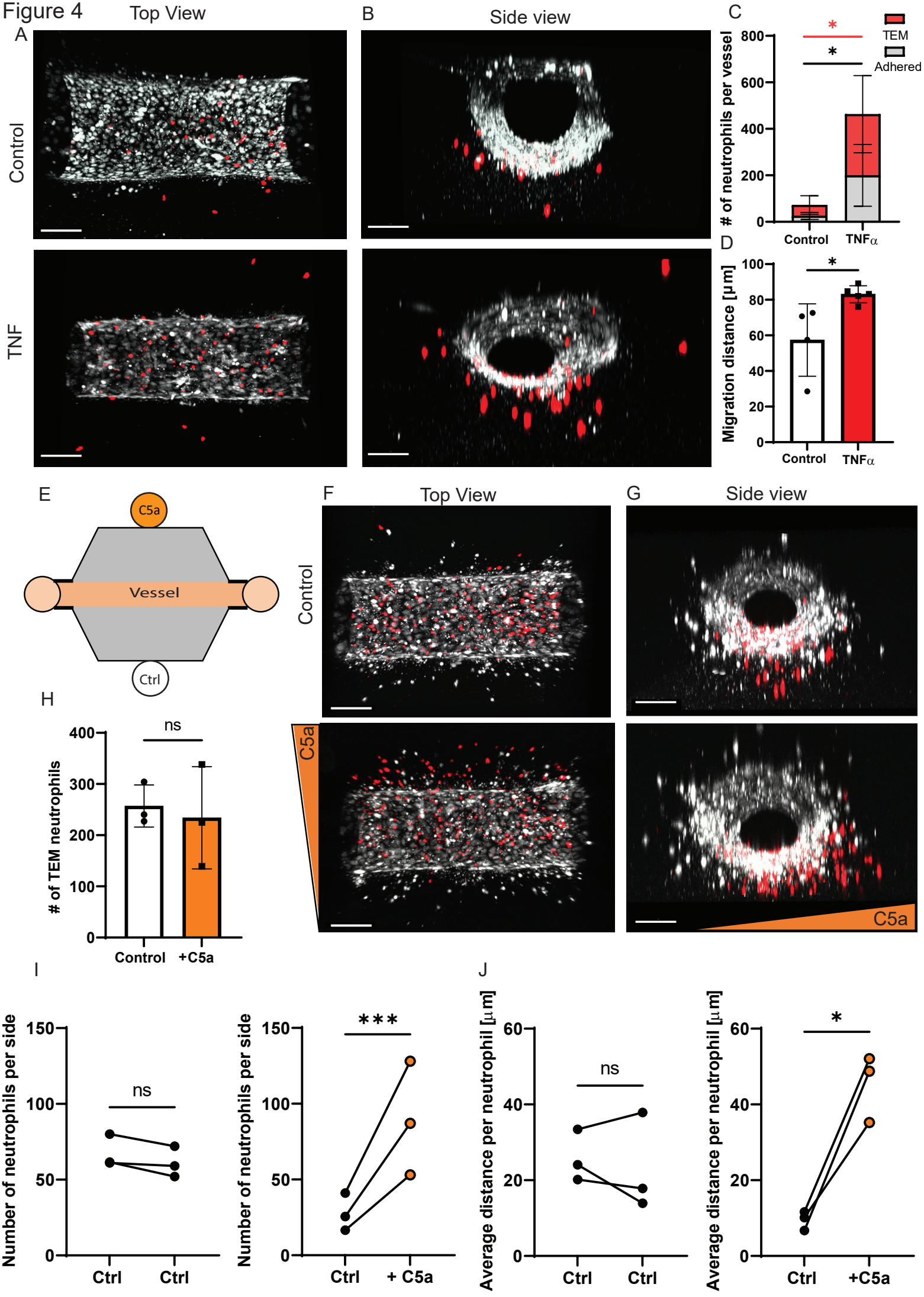
A
Top View
B
Side view
C
Control
TNF
TEM
Adhered
# of neutrophils per vessel
Control
TNFα
D
Migration distance [µm]
Control
TNFα
E
C5a
Vessel
Ctrl
F
Top View
G
Side view
Control
C5a
C5a
H
ns
# of TEM neutrophils
Control
+C5a
I
Number of neutrophils per side
ns
Ctrl
Ctrl
***
Ctrl
+ C5a
J
Average distance per neutrophil [µm]
ns
Ctrl
Ctrl
Average distance per neutrophil [µm]
Ctrl
+C5a

Figure 5

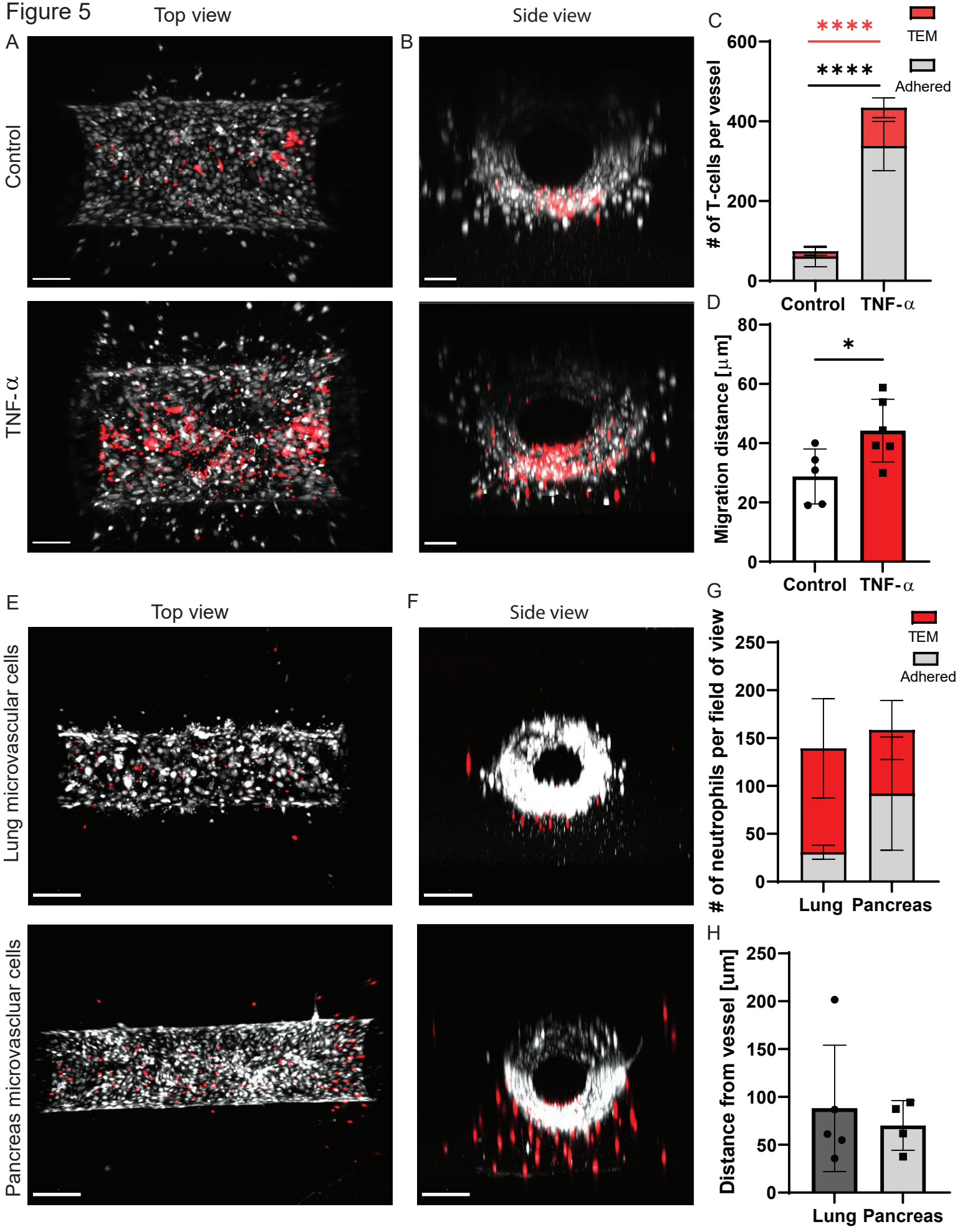
Top view
Side view
A
B
Control
TNF-α
C
****
****
TEM
Adhered
# of T-cells per vessel
600
400
200
0
Control
TNF-α
D
*
Migration distance [μm]
80
60
40
20
0
Control
TNF-α
E
Top view
F
Side view
Lung microvascular cells
Pancreas microvascular cells
G
TEM
Adhered
# of neutrophils per field of view
250
200
150
100
50
0
Lung
Pancreas
H
Distance from vessel [um]
250
200
150
100
50
0
Lung
Pancreas

Figure 6

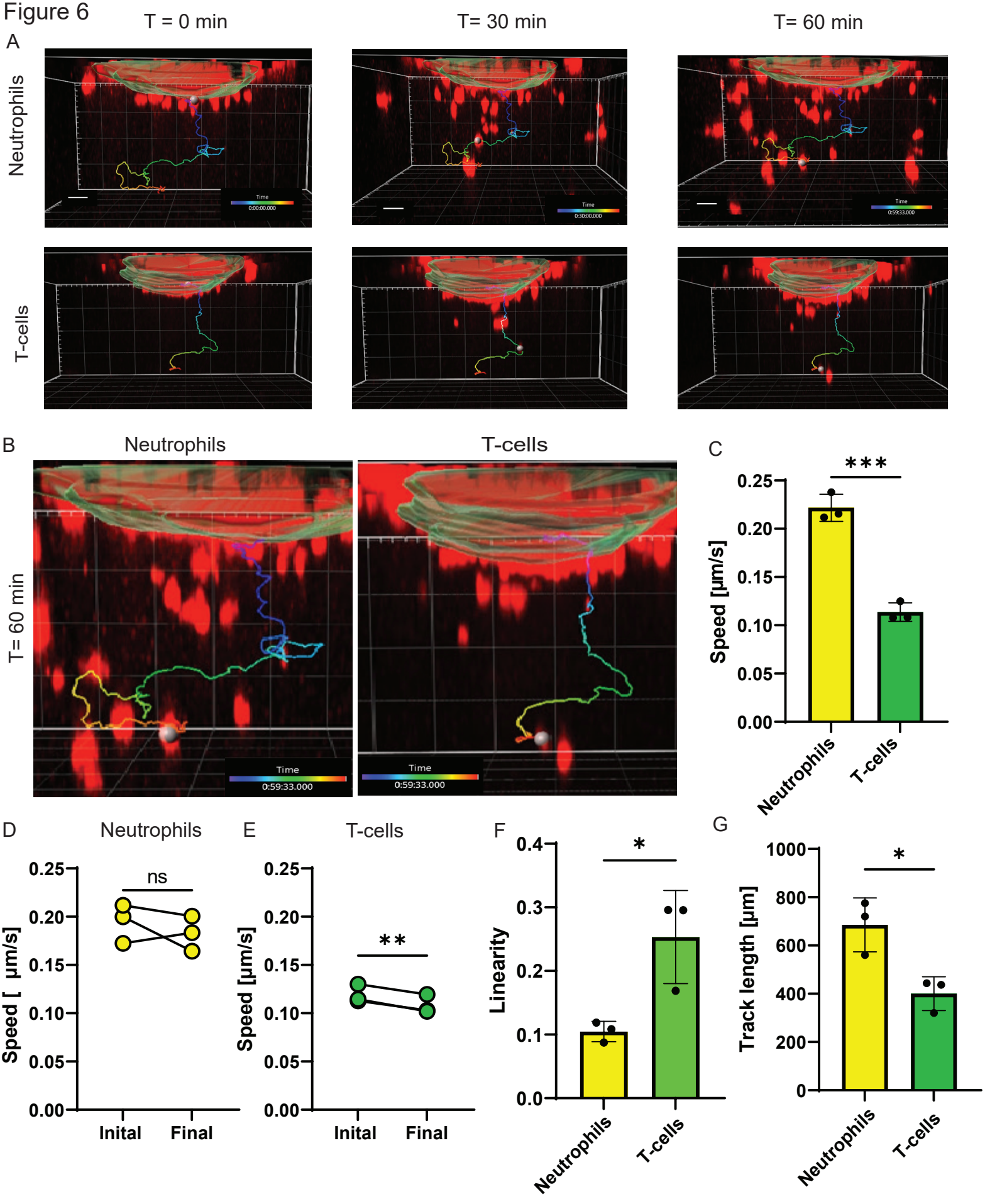
A
T = 0 min
T= 30 min
T= 60 min
Neutrophils
T-cells
B
Neutrophils
T-cells
T= 60 min
Time
0:59:33.000
C
***
Speed [µm/s]
0.25
0.20
0.15
0.10
0.05
0.00
Neutrophils
T-cells
D
Neutrophils
ns
Speed [µm/s]
Inital
Final
E
T-cells
**
Speed [µm/s]
Inital
Final
F
*
Linearity
0.4
0.3
0.2
0.1
0.0
Neutrophils
T-cells
G
*
Track length [µm]
1000
800
600
400
200
0
Neutrophils
T-cells

Figure 7

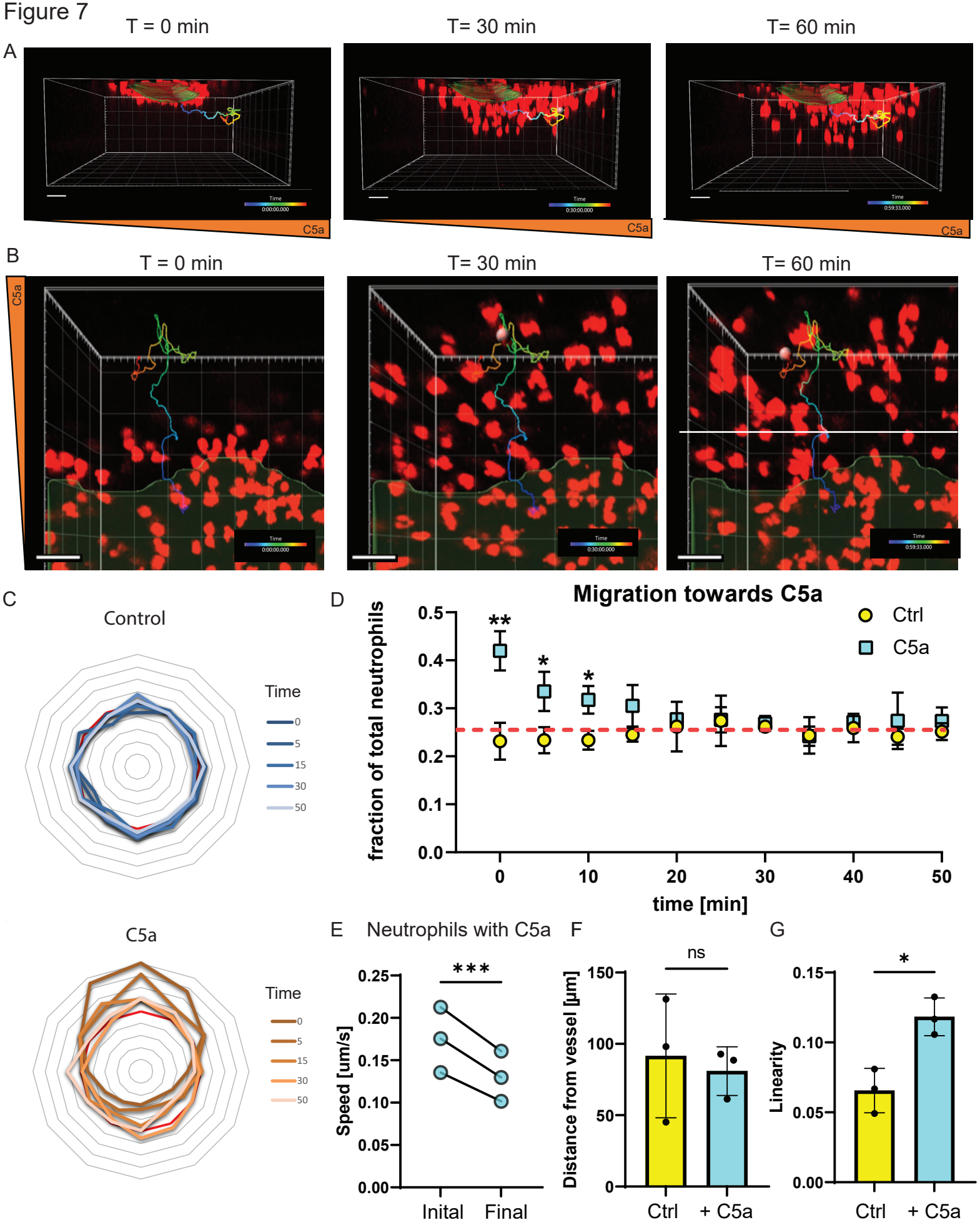
A
T = 0 min
T= 30 min
T= 60 min
C5a
B
T = 0 min
T= 30 min
T= 60 min
C5a
C
Control
Time
0
5
15
30
50
C5a
Time
0
5
15
30
50
D
Migration towards C5a
Ctrl
C5a
fraction of total neutrophils
time [min]
0.0
0.1
0.2
0.3
0.4
0.5
0
10
20
30
40
50
**
*
*
E
Neutrophils with C5a
***
Speed [um/s]
0.00
0.05
0.10
0.15
0.20
0.25
Inital
Final
F
ns
Distance from vessel [µm]
0
50
100
150
Ctrl
+ C5a
G
*
Linearity
0.00
0.05
0.10
0.15
Ctrl
+ C5a

Figure 8

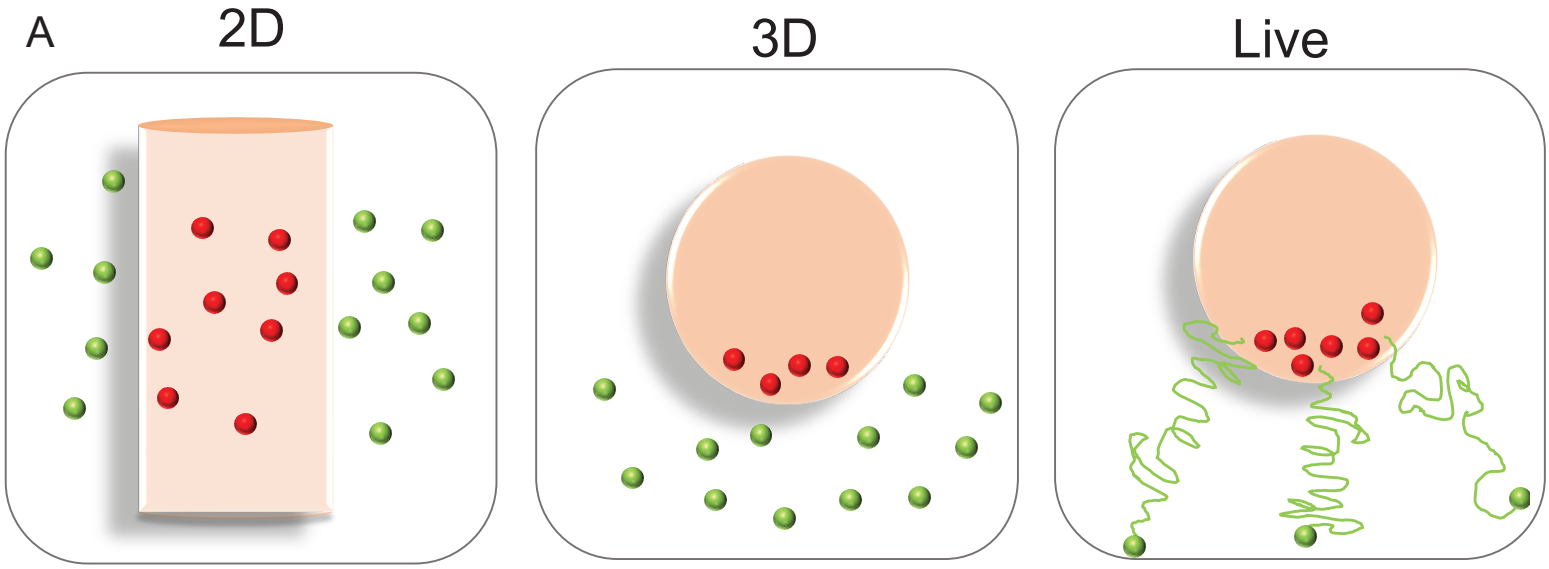
A
2D
3D
Live

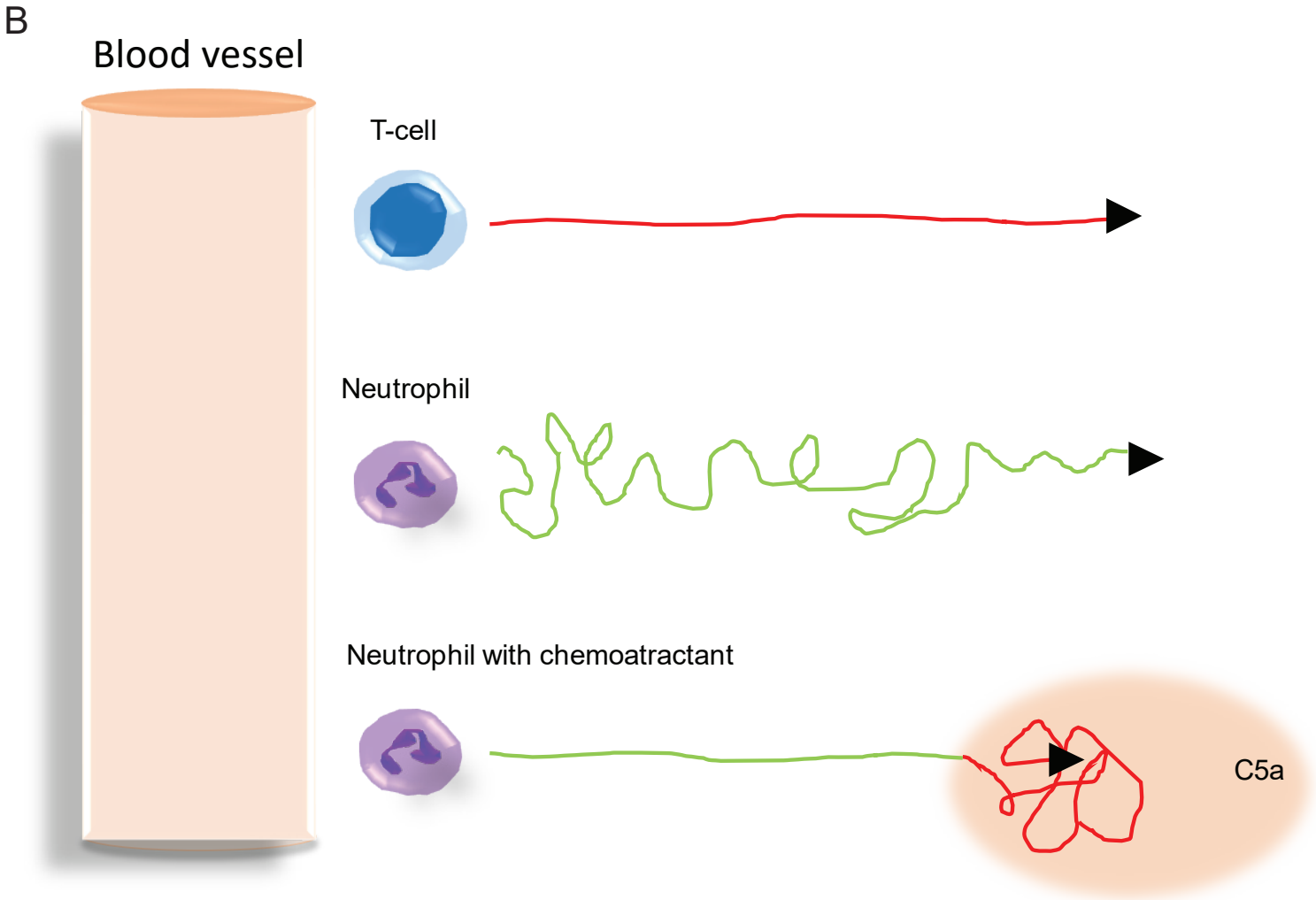
B
Blood vessel
T-cell
Neutrophil
Neutrophil with chemoatractant
C5a